Multipolar x-ray diffraction study of the canted magnetic structure of TbMg

2002 J. Phys.: Condens. Matter 14 935

(http://iopscience.iop.org/0953-8984/14/4/325)

INSTITUTE OF PHYSICS PUBLISHING JOURNAL OF PHYSICS: CONDENSED MATTER

J. Phys.: Condens. Matter **14** (2002) 935–944 PII: S0953-8984(02)28503-3

Multipolar x-ray diffraction study of the canted magnetic structure of TbMg

S E Luca[1], M Amara[1,3], R M Galéra[1] and J F Bérar[2]

[1] Laboratoire Louis-Néel[4], CNRS, BP 166X, F-38042 Grenoble, France
[2] Laboratoire de Cristallographie[4], CNRS, BP 166X, F-38042 Grenoble, France

E-mail: amara@polycnrs-gre.fr

Received 3 September 2001
Published 18 January 2002
Online at stacks.iop.org/JPhysCM/14/935

Abstract

Earlier neutron powder diffraction measurements on the CsCl compound TbMg showed that a canted magnetic structure is stabilized at $T = 4.2$ K. This structure mixes ferromagnetic and antiferromagnetic, $\langle \frac{1}{2}\,0\,0 \rangle$, components. Accounting for the anisotropy, several consistent models of structures could be proposed. In order to identify the best one, we performed x-ray diffraction measurements on a single crystal. A set of charge satellites originating from multipolar 4f scattering and related to the $\langle \frac{1}{2}\,0\,0 \rangle$ wavevectors were observed. Analysing the experimental data, within the framework recently proposed for multipolar scattering in cubic systems, a model is selected for the magnetic structure of TbMg.

1. Introduction

We have in recent papers discussed the relation between the magnetic structure and 4f multipoles of second, fourth and sixth orders in rare-earth cubic systems [1, 2]. The development of the analysis, relating the asphericity of the 4f charge distribution to the magnetism, provides an alternative way to study the magnetic order by means of x-ray scattering. 4f multipolar x-ray scattering has the considerable advantage, as compared with x-ray magnetic scattering, of significant scattering amplitudes. Using NdMg as a test compound, we showed that these intensities can be measured within reasonable counting times, despite the intrinsic weakness of the neodymium multipolar scattering amplitudes [3]. However, as the relation between charge and magnetic order is not bijective, the multipolar structure that may actually be determined is in general consistent with several magnetic models. Therefore, multipolar x-ray scattering cannot be used alone for a magnetic structure determination. This requires prior knowledge of the magnetic wavevector, and then allows one to select the best among several magnetic models. For rare-earth ions with large multipolar

[3] Author to whom any correspondence should be addressed.
[4] Associated with the Joseph Fourier University of Grenoble.

0953-8984/02/040935+10$30.00

scattering amplitudes, such as Tb^{3+}, this technique may become a valuable alternative to the neutron scattering technique for single crystal. Indeed, in some cases neutron studies may be too delicate due, for instance, to absorption problems or to difficulties in obtaining large enough single crystals.

TbMg appeared to us a very suitable system for testing the x-ray multipolar scattering technique applied to the determination of a magnetic structure. Earlier neutron powder diffraction experiments showed the existence at low temperature of a canted magnetic structure, with antiferromagnetic wavevectors from the $\langle \frac{1}{2}\,0\,0\rangle$ star. Several models were found to be consistent with experiments and the actual structure remained undetermined. Moreover, the compounds in the rare-earth magnesium series show an unusual, among rare-earth intermetallics, reluctance to oxidize. This reduces the contribution of the oxidized surface to the scattering phenomena and favours the observation of weak multipolar reflections.

In the following, we first recall the magnetic properties of TbMg and the models of magnetic structures consistent with the neutron powder diffraction experiment. Second, we present our x-ray scattering experiments, their results and subsequent analysis.

2. TbMg: the current state of knowledge

2.1. Magnetic order in R–Mg compounds

TbMg belongs to the same series of CsCl compounds as the multiaxial antiferromagnet NdMg. Unlike the latter, however, TbMg is reported to order not antiferromagnetically, but ferromagnetically at $T_C = 81$ K [4]. It turns out that this follows a trend in the series, in which elements with light rare earths order antiferromagnetically, whereas the ones with heavy rare earths, including TbMg, exhibit a Curie temperature [4,5]. There are, however, the exceptions of DyMg and TmMg; DyMg is reported to be an antiferromagnet, whereas for TmMg no order was observed down to 1.5 K [6]. For the ferromagnetic elements, the antiferromagnetic couplings remain competitive and, at low temperature, canted structures mixing ferromagnetic and antiferromagnetic components were proposed for GdMg, TbMg, HoMg and ErMg. For GdMg and TbMg this was supported by powder neutron diffraction results at $T = 4.2$ K [7,8], which showed the existence of $\langle \frac{1}{2}\,0\,0\rangle$ antiferromagnetic wavevectors. Such canted magnetic structures cannot be explained within the framework of isotropic bilinear exchange associated with, in the case of TbMg, magnetocrystalline anisotropy. Bilinear exchange requires that the magnetic wavevectors correspond, at the transition temperature, to the maximum of the magnetic coupling dispersion curve, in agreement with the susceptibility $\chi(q)$ of the conduction electrons which mediate the interactions. In the case of antiferromagnetic structures with long periods, additional harmonics wavevectors may appear while decreasing the temperature, to 'square up' the structure. Obviously, such a mechanism cannot apply for the simple $\langle \frac{1}{2}\,0\,0\rangle$ wavevectors in TbMg and GdMg. The simultaneous observation of ferromagnetism and antiferromagnetism would then need the bilinear dispersion curve to take the same value at two non-equivalent points of the reciprocal lattice, [0 0 0] and $[\frac{1}{2}\,0\,0]$. This would be a very striking coincidence, and a more reasonable way to explain the occurrence of those structures is on the basis of the interference of additional pair interactions in the Hamiltonian of the system. Considering anisotropic bilinear exchange couplings appears to be insufficient for explaining the occurrence of a canted structure down to 0 K [9]. As for other kinds of multiaxial structure, the stabilization of a canted structure may be ascribed to the interference of quadrupolar pair interactions. The associated energy terms are of higher order than the bilinear interaction ones. Therefore, in the case of a second-order phase transition, they cannot interfere at T_C, but become relevant with the increase of the magnetic order

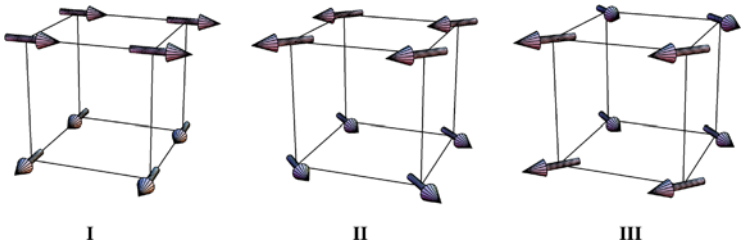

Figure 1. Sketches of the high-symmetry models of the structure, I, II and III, compatible with the $T = 4.2$ K powder neutron diffraction results for TbMg.

parameter. Then, the system undergoes a second transition which brings in an additional, antiferromagnetic, component. Such a mechanism has been proposed for the canted structure of the NaCl-type compound HoP [9].

In the case of the gadolinium S state, one would expect all orbital couplings to cancel. Nevertheless, even in this particular case, orbital contributions to the interaction energy can exist due to the orbital character of the conduction electrons involved in the RKKY coupling [9]. Consequently, a scenario similar to that for HoP can develop in gadolinium compounds. This has been confirmed for GdMg, by means of powder neutron diffraction measurements at variable temperature [7], as well as specific heat measurements [10]. Indeed, in GdMg, the antiferromagnetic component does not appear at $T_C = 110$ K but at $T_{cant} = 85$ K.

Equivalent experimental studies are lacking for the case of TbMg and the occurrence of a second phase transition at T_{cant}, related to the emergence of the antiferromagnetic component, is not supported. As terbium has a large orbital momentum, quadrupolar couplings should play a significant role, as in HoP, in the stabilization of the canted magnetic structure. Prior to developing such a quadrupolar interactions analysis for TbMg, all uncertainties about the low-temperature magnetic structure of this compound have to be removed. In view of this, one can take advantage of the large orbital moment of terbium in performing x-ray multipolar scattering experiments.

2.2. Magnetic models for the low-temperature state of TbMg

Let us first recall the results of the powder neutron diffraction experiments. For $T = 4.2$ K, the spectra show the coexistence of ferromagnetism with antiferromagnetism associated with wavevectors from the $\langle \frac{1}{2}\,0\,0 \rangle$ star. At this temperature, the ferromagnetic and antiferromagnetic amplitudes represent 5.2 μ_B per terbium, the antiferromagnetic component(s) being perpendicular to its (their) wavevector(s). At this rather low temperature, in order to minimize the bilinear interaction energy for the commensurate wavevectors involved, $\boldsymbol{q} = \mathbf{0}$ and $\boldsymbol{q} \in \langle \frac{1}{2}\,0\,0 \rangle$, the moments should be of identical (maximum) amplitude on all sites. In addition, due to the non-zero orbital moment of terbium, the magnetic moment directions should follow the crystal-field anisotropy and, therefore, belong to a unique crystallographic star compliant with the cubic system ($\langle 100 \rangle$, $\langle 110 \rangle$ or $\langle 111 \rangle$).

According to these criteria, only three magnetic structures can be retained, referred to as I, II and III (an exhaustive list of these models mixing antiferromagnetic, $\langle \frac{1}{2}\,0\,0 \rangle$, and ferromagnetic components can be found in [11]). These three structures are represented in figure 1 and their respective Fourier descriptions detailed in table 1.

Given the Fourier description of a high-symmetry magnetic structure, the method presented in [2] allows the determination of its 4f multipolar counterpart. That is, one can determine which multipolar components should be non-zero and their associated wavevectors.

Table 1. Fourier description of the structure models proposed for TbMg in terms of magnetic, quadrupolar, hexadecapolar and hexacontatetrapolar components. The total magnetic moment amplitude is one unit. The only difference between models II and III lies in the association between the antiferromagnetic component and the $\langle \frac{1}{2}\,0\,0\rangle$ wavevector.

Model	Wavevectors	Magnetic	Quadrupolar	Hexadecapolar	Hexacontatetrapolar
I	[0 0 0]	$(\frac{1}{2}\ \frac{1}{2}\ 0)$	$\langle O_2^0\rangle$	$\langle O_4^{\gamma,1}\rangle$	$\langle O_6^{\gamma,1}\rangle$
	$[0\,0\,\frac{1}{2}]$	$(\frac{1}{2}\ -\frac{1}{2}\ 0)$	$\langle O_2^2\rangle$	$\langle O_4^{\gamma,2}\rangle$	$\langle O_6^{\gamma,2}\rangle$
II	[0 0 0]	$(\frac{1}{\sqrt{2}}\,0\,0)$	$\langle O_2^0\rangle$	$\langle O_4^{\gamma,1}\rangle$	$\langle O_6^{\gamma,1}\rangle$
	$[0\,0\,\frac{1}{2}]$	$(0\ \frac{1}{\sqrt{2}}\ 0)$	$\langle P_{xy}\rangle$	$\langle O_4^{\varepsilon,1}\rangle$	$\langle O_6^{\varepsilon_1,1}\rangle$, $\langle O_6^{\varepsilon_2,1}\rangle$
III	[0 0 0]	$(\frac{1}{\sqrt{2}}\,0\,0)$	$\langle O_2^0\rangle$	$\langle O_4^{\gamma,1}\rangle$	$\langle O_6^{\gamma,1}\rangle$
	$[\frac{1}{2}\,0\,0]$	$(0\,\frac{1}{\sqrt{2}}\,0)$	$\langle P_{xy}\rangle$	$\langle O_4^{\varepsilon,1}\rangle$	$\langle O_6^{\varepsilon_1,1}\rangle$, $\langle O_6^{\varepsilon_2,1}\rangle$

The results of this analysis applied to the three magnetic models are reported in table 1. The listed, ordered, cubic multipolar components match the definitions given by Morin and Schmitt [12]. Due to the presence in all the magnetic models of a single $\langle \frac{1}{2}\,0\,0\rangle$ wavevector, the only zone-boundary 4f charge wavevector is identical to this antiferromagnetic one. This is in contrast with the NdMg multiaxial structure for which two antiferromagnetic $\langle \frac{1}{2}\,0\,0\rangle$ wavevectors result in a single zone-boundary, $\langle \frac{1}{2}\ \frac{1}{2}\ 0\rangle$, charge wavevector. As regards the use of multipolar x-ray diffraction, one can expect to observe charge satellites for scattering vectors of the $\{\frac{1}{2}(2n+1)\ m\ p\}$ type, where (n, m, p) are integers. Confusion of such charge reflections with magnetic ones is highly unlikely because the multipolar reflections are three or four orders of magnitude larger than the non-resonant magnetic x-ray ones [1]. At this point, the observation of such $\{\frac{1}{2}(2n+1)\ m\ p\}$ charge satellites is not selective as regards the magnetic models and a more detailed analysis of the multipolar scattering is necessary. This is achieved by writing down the multipolar scattering amplitudes for the three models, according to the expressions given in [2]. These scattering amplitudes are reported in table 2. Model I has ordered $\langle \frac{1}{2}\,0\,0\rangle$ multipolar components of the Γ_3 type and therefore fundamentally differs from models II and III, whose $\langle \frac{1}{2}\,0\,0\rangle$ ordered multipoles are of the Γ_5 type. This difference manifests itself in the conditions of existence for the reflections reported in the last column of table 2. The distinction between models II and III is more delicate, since they have common Γ_5-type ordered components. However, they differ in the association of these components with the $\langle \frac{1}{2}\,0\,0\rangle$ wavevector. According to the existence conditions reported in the last column of table 2, for integers m and n:

(i) $\{\frac{1}{2}(2n+1)\,0\,0\}$ reflections cancel for all the three models;
(ii) $\{\frac{1}{2}(2n+1)\,m\ \pm m\}$ reflections cancel for model I only;
(iii) $\{\frac{1}{2}(2n+1)\,m\,0\}$ reflections cancel for model II but not for model III (if all domains are present).

It should be then possible to identify the real structure by measuring a set of reflections in which these three groups would be represented.

Note that, as regards the 4f charge, the three models determine a tetragonal symmetry lowering related to the emergence of $\Gamma_3(\gamma)$ multipolar components at the zone centre (table 1). The magnetoelastic couplings will force a spontaneous magnetostriction of the same symmetry, that is a tetragonal strain mode ε_1^{γ} [12]. Obviously, as this behaviour is common to all three models, magnetostriction measurements cannot help to distinguish between them. If the magnetoelastic couplings are strong enough, they should determine a splitting of the lattice reflections within the ordered range, as has been observed for NdMg [3].

Table 2. Multipolar x-ray scattering amplitudes and reflection conditions for the particular domains representing models I, II and III here. $\boldsymbol{Q} = [h\,k\,l]$ is the scattering vector. α_J, β_J and γ_J are the Stevens multiplication factors [13]. $F_2(Q)$, $F_4(Q)$ and $F_6(Q)$ are the second-, fourth- and sixth-order multipolar scattering form factors [1].

Model, wavevector	Multipolar x-ray scattering amplitude	Condition
I, $[0\,0\,\frac{1}{2}]$	$(h^2-k^2)\left\{\begin{array}{l}\frac{3}{2}\frac{\alpha_J F_2(Q)}{Q^2}\langle O_2^2\rangle + \frac{5}{8\sqrt{3}}\frac{\beta_J F_4(Q)}{Q^4}(Q^2-7l^2)\langle O_4^{\gamma,2}\rangle \\ \quad + \frac{7\sqrt{3}}{16}\frac{\gamma_J F_6(Q)}{Q^6}(Q^4-7Q^2l^2+11l^4-11h^2k^2)\langle O_6^{\gamma,2}\rangle\end{array}\right\}$	$l=(2n+1)/2$, and $h^2\neq k^2$
II, $[0\,0\,\frac{1}{2}]$	$hk\left\{\begin{array}{l}6\frac{\alpha_J F_2(Q)}{Q^2}\langle P_{xy}\rangle + 5\frac{\beta_J F_4(Q)}{Q^4}(7l^2-Q^2)\langle O_4^{\varepsilon,1}\rangle \\ \quad + \frac{\gamma_J F_6(Q)}{Q^6}\left[\frac{105}{16}(33l^4-18Q^2l^2+Q^4)\langle O_6^{\varepsilon_1,1}\rangle\right. \\ \quad \left. + \frac{231}{32}(3h^4-10h^2k^2+3k^4)\langle O_6^{\varepsilon_2,1}\rangle\right]\end{array}\right\}$	$l=(2n+1)/2$ and $hk\neq 0$
III, $[\frac{1}{2}\,0\,0]$	$hk\left\{\begin{array}{l}6\frac{\alpha_J F_2(Q)}{Q^2}\langle P_{xy}\rangle + 5\frac{\beta_J F_4(Q)}{Q^4}(7l^2-Q^2)\langle O_4^{\varepsilon,1}\rangle \\ \quad + \frac{\gamma_J F_6(Q)}{Q^6}\left[\frac{105}{16}(33l^4-18Q^2l^2+Q^4)\langle O_6^{\varepsilon_1,1}\rangle\right. \\ \quad \left. + \frac{231}{32}(3h^4-10h^2k^2+3k^4)\langle O_6^{\varepsilon_2,1}\rangle\right]\end{array}\right\}$	$h=(2n+1)/2$ and $k\neq 0$

3. X-ray diffraction experiment

3.1. Experimental conditions

Unlike the R–Mg compounds with light rare earths (R), the heavy-rare-earth ones melt incongruently and the TbMg crystals which were available at the start of this study were of too poor a quality (inclusions of $TbMg_2$) for any neutron or x-ray scattering study. New attempts at synthesis were performed in order to obtain crystals of sufficient quality and size for the x-ray scattering study. The sample used in this experiment is part of an ingot processed by the Bridgman technique in a sealed tantalum crucible. In order to start the solidification at about the peritectic point of TbMg, the starting concentration was shifted from stoichiometry according to the metallurgical phase diagram published by Saccone *et al* [14]. The Lauë patterns showed that the tip of the ingot was a well crystallized single crystal, but that on going along the ingot the quality decreased rapidly. Optical microscopy showed that this deterioration was related to the presence of inclusions growing dendritically which, according to the phase diagram, should be of $TbMg_2$. A small single crystal was spark cut out of the tip and shaped into a fairly rectangular plate of dimensions $5 \times 3 \times 0.5$ mm^3. The 5×3 mm^2 surface later exposed to the x-ray beam is perpendicular to a fourfold axis. To remove any defect arising from the spark cutting, as well as oxide, this surface was chemically polished using an ethanol solution of nitric acid. The quality of the surface was then checked by means of Lauë patterns.

In the case of NdMg, it appeared that the partitioning of the sample into domains was critical as regards the intensities of the reflections. In order to avoid dispersion of the scattered intensities over all the $\langle\frac{1}{2}\,0\,0\rangle$ branches and, also, to simplify the analysis, we decided to take advantage of the ferromagnetic component of the structure for selecting domains. To achieve this domain selection, the sample was glued such that it closed a small magnetic circuit consisting in two soft iron pieces and a $Nd_2Fe_{14}B$ magnet (inset of figure 2). The field thus applied to the sample was directed along the [1 0 0] fourfold direction which approximately corresponds to its largest dimension. The efficiency of this magnetic circuit was checked by zero-field magnetization measurements under variable temperature (figure 2). If the TbMg sample is not saturated by the field, its contribution to the magnetic circuit's dipole is governed by the demagnetizing effect. Therefore, this contribution is essentially shape dependent but

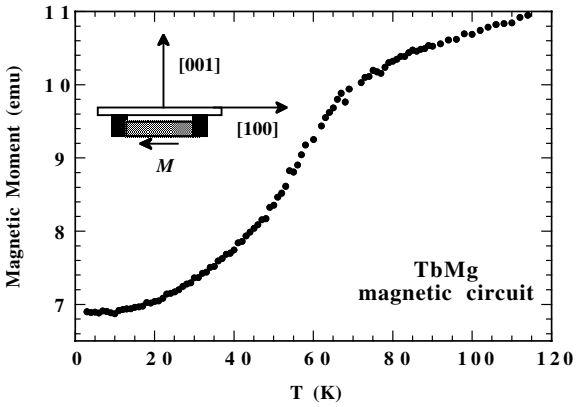

Figure 2. The thermal dependence of the sample's magnetic circuit moment along the [1 0 0] direction. Inset: a sketch of the sample's magnetic circuit with: in grey, the $Nd_2Fe_{14}B$ magnet of magnetization M; in black, the soft iron pieces; and, in white, the TbMg single crystal with its [1 0 0] and [0 0 1] reference directions.

not temperature dependent (in this temperature range, the thermal dependence of the $Nd_2Fe_{14}B$ magnetization can be neglected). Experimentally, the observed decrease of the magnetic circuit dipole, below T_C, seems to follow the thermal dependence of the ferromagnetic component of TbMg. This, together with the still huge leakage of the circuit at low temperature, is indicative of the magnetically saturated state of the sample at all temperatures below T_C. Thus, one can safely consider that at the centre of the sample, exposed to x-rays, the remaining domains are those favoured by the applied field.

The x-ray experiment was performed at the ESRF, BM2 beamline, using the seven-circle goniometer and a closed-cycle helium refrigerator for adjusting the sample temperature between 21 and 300 K. As very weak scattering intensities had to be measured, the signal-to-background ratio had to be optimized. In view of this, an x-ray wavelength $\lambda = 1.0912$ Å—and thus a photon energy far above the terbium $L_{2,3}$ absorption edges—was used. The size of the incident x-ray beam, at the sample's position, was less than 0.1 mm^2. A Ge(111) analyser was mounted in front of the detector, both to decrease the background level and to improve the q-space resolution of the experiments. This latter precaution avoids the spreading of strong parasitic reflections from the sample surface which could hide the multipolar reflections. The sample was mounted in the refrigerator with the [0 0 1] axis vertical for zero θ- and χ-angles (inset of figure 2). The [1 0 0] direction corresponded to the field provided by the magnetic circuit, this direction being perpendicular to the incident beam for zero azimuthal ϕ-angle. Within these orientation conditions, for an effective domain selection, new restrictive conditions for the existence of $\langle \frac{1}{2}\, 0\, 0 \rangle$ multipolar reflections could be established. They appear in table 3 together with the zone-boundary wavevectors of the field-selected domains for the three models of the structure.

3.2. Measurements

At $T = 21$ K, scanning lattice reflections such as [0 0 4], [3 0 3] and [2 $\bar{2}$ 2], it appeared that the low-temperature strain was not large enough to resolve the peaks associated with the different, presumed tetragonal, domains. Consequently, a low-temperature orientation matrix was established, considering the crystallographic system as still cubic. Thereafter, we proceeded by testing the accessibility and background level for $\{\frac{1}{2}(2n+1)\, m\ p\}$ scattering vectors. This was done in order to establish a list of multipolar reflections which could be measured with

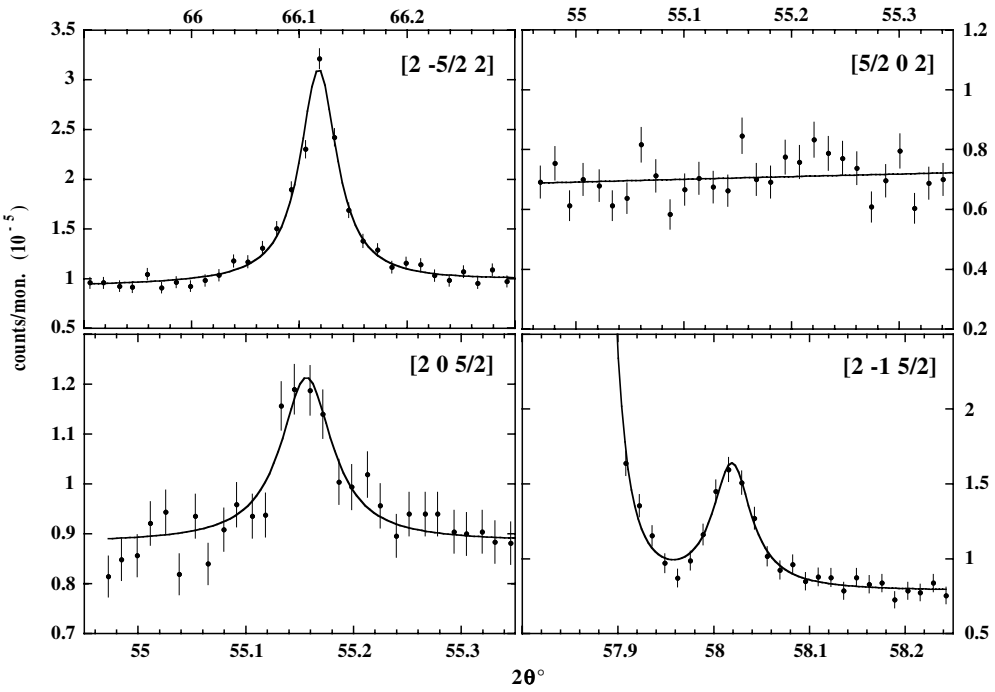

Figure 3. Some illustrative examples of $(\theta, 2\theta)$ scans across $\{\frac{1}{2}(2n+1)\,m\,p\}$ positions. The full curves are Lorentzian fits (whenever possible). Reflection $[2\,\bar{1}\,\frac{5}{2}]$ illustrates the difficulty of measuring such weak charge satellites in the vicinity of parasitic reflections from the sample's surface.

Table 3. Reflection conditions, for a scattering vector $\boldsymbol{Q} = [h\,k\,l]$, according to the three models and for the domains selected by a magnetic field applied along [1 0 0]. n is an integer and 'XOR' stands for 'exclusive or'.

Model	Wavevector	Number of domains	Reflection if:
I	$[0\,0\,\frac{1}{2}]$	2	$l = (2n+1)/2$ and $h^2 \neq k^2$
	$[0\,\frac{1}{2}\,0]$	2	$k = (2n+1)/2$ and $h^2 \neq l^2$
II	$[0\,0\,\frac{1}{2}]$	1	$k = (2n+1)/2$ and $hl \neq 0$
	$[0\,\frac{1}{2}\,0]$	1	$l = (2n+1)/2$ and $hk \neq 0$
III	$[\frac{1}{2}\,0\,0]$	2	$h = (2n+1)/2$ and $(k \neq 0$ XOR $l \neq 0)$

reasonable counting times thanks to a good enough signal-to-noise ratio. The expected intensities for multipolar reflections are five orders of magnitude smaller than for standard lattice ones. A typical lattice reflection, $[2\,\bar{2}\,2]$, represents 4.5×10^5 counts s^{-1} at the peak's maximum. Thus, one could expect a few counts per second for a multipolar peak and the positions retained were the ones with background level less than 3 counts s^{-1}. Thereafter, $(\theta, 2\theta)$ scans with long acquisition times were measured across these positions. Due to the ω-extension of the Bragg reflections, this $(\theta, 2\theta)$ type of scan was chosen to improve the contrast with respect to the background. Obviously, this does not allow a rigorous quantitative analysis, but our main purpose was to check whether these reflections did or did not exist. Some illustrative examples of these scans are given in figure 3 and their results are condensed in table 4, where they can be compared with the predictions for the three models. The reported

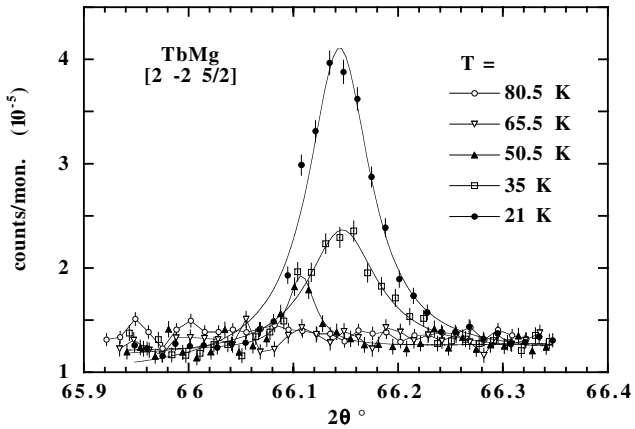

Figure 4. The thermal dependence of the $[2\,\bar{2}\,\frac{5}{2}]$ multipolar reflection as observed through $(\theta, 2\theta)$ scans. Lorentzian fits, shown as full curves, are superimposed on the $T = 21$, 35 and 50.5 K data.

amplitudes (peak maximum) result from Lorentzian fits and are indicative of the reflection intensities. It appears that the best agreement is obtained for model II for which the experiment matches the prediction for 11 scans out of 13. Moreover, the unexpected reflections, $[1\,0\,\frac{5}{2}]$ and $[2\,0\,\frac{5}{2}]$, are the weakest among the non-zero ones.

The temperature dependence of the $[2\,\bar{2}\,\frac{5}{2}]$ reflection was measured starting from 21 K and warming up to 80 K. In order to compensate for a possible discrepancy between the $T = 21$ K orientation matrix and the lattice at higher temperatures, the position of the $[2\,\bar{2}\,\frac{5}{2}]$ satellite was checked prior to the measurements by centring the $[2\,\bar{2}\,2]$ and $[2\,\bar{2}\,3]$ reflections. The corresponding scans are shown in figure 4. Considering the value $T = 81$ K of the ordering temperature the intensity of the reflection drops rapidly when increasing the temperature. Indeed, the reflection is almost zero at $T = 50.5$ K and cannot be distinguished from the background at $T = 65.6$ K. A small shift of the $T = 50.5$ K peak maximum can be ascribed to a deviation of the antiferromagnetic wavevector from the commensurate $\langle \frac{1}{2}\,0\,0 \rangle$ star. As expected, no intensity is measured at $T = 80.5$ K, as one reaches the paramagnetic phase.

4. Discussion

This x-ray experiment has provided reliable evidence in favour of model II, proposed for the TbMg low-temperature magnetic structure, even if this model does not reach 100% agreement with the experiment. Some hypotheses may be put forward regarding the existence of two ($[1\,0\,\frac{5}{2}]$ and $[2\,0\,\frac{5}{2}]$) unexpected reflections for model II:

(a) Magnetic x-ray scattering.
(b) A contamination by higher-order harmonics from the monochromator.
(c) An imperfect domain selection by the field provided by the magnetic circuit.
(d) A deviation of the structure from the high-symmetry model.

Hypothesis (a) can be ruled out easily as the intensities for reflections $[1\,0\,\frac{5}{2}]$ and $[2\,0\,\frac{5}{2}]$ are only one order of magnitude smaller than the maximum intensity obtained for $[2\,\bar{2}\,\frac{5}{2}]$. Thus, one would have to consider that these supposed magnetic reflections reach 10^{-6} times the intensity of a standard lattice reflection. The strong amplitude of this off-resonance magnetic scattering phenomenon would be totally unexplained. In the similar case of NdMg, our attempts

Table 4. Semi-quantitative comparison between the multipolar Bragg reflection measurements and the predictions for models I, II and III. The measured amplitudes are reported in units of 10^{-5} counts per detector/monitor, the uncertainty being ± 0.1. '**X**' indicates the existence of a reflection (predicted or measured) and '—' an extinction (a predicted extinction or no identifiable experimental peak). The last line gives the ratio of coincidences with the experiment for the three models.

$[h\,k\,l]$	Amplitude	Existence	I	II	III
$[2\,\bar{2}\,\frac{5}{2}]$	3	**X**	—	**X**	—
$[0\,0\,\frac{5}{2}]$	<0.1	—	—	—	—
$[1\,0\,\frac{5}{2}]$	0.35	**X**	**X**	—	—
$[0\,\bar{1}\,\frac{5}{2}]$	<0.1	—	**X**	—	—
$[2\,0\,\frac{5}{2}]$	0.35	**X**	**X**	—	—
$[0\,\bar{2}\,\frac{5}{2}]$	<0.1	—	**X**	—	—
$[2\,\bar{1}\,\frac{5}{2}]$	0.8	**X**	**X**	**X**	—
$[1\,\bar{1}\,\frac{3}{2}]$	0.75	**X**	—	**X**	—
$[2\,\bar{\frac{5}{2}}\,2]$	2.2	**X**	**X**	**X**	—
$[1\,\frac{5}{2}\,3]$	0.7	**X**	**X**	**X**	—
$[0\,\frac{5}{2}\,2]$	<0.1	—	**X**	—	—
$[\frac{5}{2}\,0\,2]$	<0.1	—	—	—	**X**
$[\frac{5}{2}\,\bar{2}\,2]$	<0.1	—	—	—	**X**
	Agreement ratio (%)		61.5	84.6	30.8

to measure a magnetic reflection, for counting times equivalent to the ones devoted to the multipolar reflections, did not result in any deviation from the background [3].

At the ESRF BM2 beamline, the $\lambda/2$ contamination of the incident beam is less than 10^{-6} for the settings of the mirrors used. Moreover, the thermal dependence of the $[2\,\bar{2}\,\frac{5}{2}]$ reflection does not show any residual peak above 65.6 K. Therefore, hypothesis (b) cannot explain the occurrence of the two ($[1\,0\,\frac{5}{2}]$ and $[2\,0\,\frac{5}{2}]$) reflections.

As regards a possible interference of domains which survived the applied field, hypothesis (c): it can be checked in table 2 that reflections like $[1\,0\,\frac{5}{2}]$ and $[2\,0\,\frac{5}{2}]$ are incompatible with any domain associated with model II. Note that besides being expected for model I, these two reflections may appear in relation with domains associated with model III. In order to explain the occurrence of the two reflections $[1\,0\,\frac{5}{2}]$ and $[2\,0\,\frac{5}{2}]$, one would have to reject model II in favour of model I or III, thus accepting many contradictions for the other reflections tested.

It is difficult to find grounds for rejecting hypothesis (d). Indeed, to obtain a structure complying with the high-symmetry criteria, one would need a perfect equilibrium between the ferromagnetic and the antiferromagnetic components. This requires the antiferromagnetic and ferromagnetic couplings to be of identical strength. If not, the magnetic system will tend to favour the ferromagnetic component at the expense of the antiferromagnetic one. Despite the anisotropy, the magnetic moments of model II should then slightly deviate from the twofold directions (see figure 1). This deviation can be described by considering a canting angle between the moment direction and the fourfold axis of the magnetization, which would tend to 45° while decreasing the temperature and thus increasing the anisotropy. Such a thermal dependence for the canting angle has been observed in GdMg [7].

This deviation from the high-symmetry model will result in the emergence of additional multipolar components. At the quadrupolar level, if the magnetic moments stay in the same, say x–y, plane, one will have to consider, in addition to $\langle P_{xy} \rangle$, the emergence of an $\langle O_2^2 \rangle$

component associated with the $[0\,0\,\frac{1}{2}]$ wavevector. Obviously, the extinction rules defined for model II would not apply strictly and the observation of weak additional reflections, such as $[1\,0\,\frac{5}{2}]$ and $[2\,0\,\frac{5}{2}]$, could be expected.

The other mechanism which could give rise to weak charge satellites is the development of an atomic displacement wave [15] related to the loss of the inversion symmetry. However, this is unlikely to occur in a system for which the only definite antiferromagnetic wavevectors belong to the $\langle\frac{1}{2}\,0\,0\rangle$ star. Indeed, a phase shift is irrelevant for such a magnetic wave, as well as for a ferromagnetic one. Thus, any magnetic structure based on such components is centrosymmetric.

Another striking result of this x-ray study is the surprisingly rapid decrease of the $[2\,\bar{2}\,\frac{5}{2}]$ reflection on increasing the temperature. The main contribution to such a multipolar reflection is the quadrupolar one. As quadrupoles develop, to a first approximation, like the square of the magnetic moment, the intensity of a multipolar reflection should roughly behave as the fourth power of the magnetic order parameter. This can explain the rapid fall of the intensity of a multipolar reflection even at temperatures much lower than T_C. However, this rapid thermal variation may also reflect the existence of a second transition below T_C, associated with the emergence of the antiferromagnetic component. This would be consistent with the above comments regarding the probable distortion of the canted structure with respect to the high-symmetry model. Such a distortion is proof of an imbalance between the antiferromagnetic $\langle\frac{1}{2}\,0\,0\rangle$ and ferromagnetic bilinear exchange couplings. Thus, in case of a second-order transition at T_C, the stabilized structure should introduce only wavevectors which correspond to the maximum, here ferromagnetic, exchange coupling. Moreover, at T_C, the moment directions should comply with the cubic anisotropy which favours threefold or fourfold axes but not the twofold ones of model II. Thus, the antiferromagnetic component of model II could appear only with the interference of a competing interaction term, which would compensate for the increase of the bilinear exchange and anisotropy energies. The most serious candidates for playing this role are the quadrupolar couplings. Like the quadrupolar x-ray scattering intensity, the quadrupolar coupling energy term has a different thermal dependence to the bilinear exchange one and becomes relevant for temperatures which can be substantially lower than T_C. Thus, the system may undergo a second transition within its magnetic order range. There is no evidence that the transition at T_C is first order and this scenario is likely to apply for TbMg.

Obviously, to rigorously resolve this question, one needs a more accurate study of the thermal dependence of the $\langle\frac{1}{2}\,0\,0\rangle$ reflections. This will be achieved in due course by means of additional x-ray diffraction or magnetic neutron diffraction measurements.

References

[1] Amara M and Morin P 1998 *J. Phys.: Condens. Matter* **10** 9875
[2] Amara M, Luca S E and Galéra R M 2001 *J. Phys.: Condens. Matter* **13** 9621
[3] Amara M, Galéra R M, Morin P and Bérar J F 1998 *J. Phys.: Condens. Matter* **10** L743
[4] Buschow K H J 1973 *J. Less-Common Met.* **33** 239
[5] Aléonard R, Morin P, Pierre J and Schmitt D 1976 *J. Phys. F: Met. Phys.* **6** 1361
[6] Giraud M, Morin P, Rouchy J and Schmitt D 1986 *J. Magn. Magn. Mater.* **59** 255
[7] Morin P, Pierre J, Schmitt D and Givord D 1978 *Phys. Lett.* A **65** 156
[8] Aléonard R, Morin P, Pierre J and Schmitt D 1975 *Solid State Commun.* **17** 599
[9] Kim D and Levy M 1982 *J. Magn. Magn. Mater.* **27** 257
[10] Pierre J, Combarieu A d and Lagnier R 1979 *J. Phys. F: Met. Phys.* **9** 1271
[11] Amara M and Morin P 1995 *Physica* B **205** 379
[12] Morin P and Schmitt D 1990 *Ferromagnetic Materials* vol 5, ed K H J Buschow and E P Wohlfarth (Amsterdam: North-Holland) p 1
[13] Stevens K H W 1952 *Proc. Phys. Soc.* A **65** 209
[14] Saccone A, Delfino S, Maccio D and Ferro R 1993 *J. Phase Equil.* **4** 479
[15] Tsunoda Y, Mori M, Kumitomi N, Teraoka Y and Kanamori J 1974 *Solid State Commun.* **14** 287